Issues with the Material Point Method for geotechnical modelling, and how to address them

Augarde, Charles; Bing, Y; Charlton, T; Coombs, William M.; Brown, Michael; Brennan, Andrew

Publication date:
2018

Document Version
Peer reviewed version

Issues with the Material Point Method for geotechnical modelling, and how to address them

C.E. Augarde, Y. Bing, T.J. Charlton, W.M. Coombs, M. Cortis
Department of Engineering
Durham University, UK

M.J.Z. Brown, A. Brennan, S. Robinson.
Civil Engineering
University of Dundee, UK.

ABSTRACT: The Material Point Method (MPM) for solid mechanics was first proposed by Sulsky and co-workers in the 1990s. Since then it has been developing a growing band of followers not least because of its ability to handle large deformation problems with ease. This feature has more recently come to the notice of geotechnical researchers who have plenty of problems to solve involving large deformations. It is clear from recent publications, however, that many geotechnical researchers have found difficulties with the use of the MPM in a number of areas. In this paper we visit three of these problem areas and highlight solutions we have developed. It is to be hoped that this can remove some of the roadblocks to the use and further development of the MPM for geotechnical problems in future.

1 INTRODUCTION

The problems that have to be solved by geotechnical engineers are wide-ranging, covering tunnelling, foundations, slopes and many other areas, however there are common features of these problems that provide challenges to numerical modellers in particular. Principally these are material and geometric non-linearity. The former has been recognised as crucial for accurate modelling from before the development of computational geotechnics, in the recognition that plasticity is a vital part of any constitutive model for soil. Indeed material non-linearity is likely to feature in the majority of the papers at this conference. Geometric non-linearity has received less attention to date largely because material non-linearity is crucial to a wider range of geotechnical problems than geometric non-linearity. When using this term, we mean the ability to model large deformations and the use of strain definitions which are no longer linear with displacement, as opposed to infinitesimal strain measures for standard analyses.

The finite element method (FEM) remains the method of choice for most geotechnical numerical modelling, and with good reason. However, there are issues with its use for the class of problems mentioned above, i.e. in the modelling of large deformation problems. If large deformations are to be modelled then any mesh-based method (the FEM included) will require an update of the mesh during a stepped non-linear solve to avoid the inaccuracies associated with distorted elements. Any change of mesh will then require a mapping of state variables from the old to the new mesh. While both of these actions bring potential errors the FEM has been successfully adapted for large deformation problems via modifications such as the Arbitrary Lagrangian Eulerian (ALE) method and there are other examples which do much the same thing, such as the Coupled Eulerian-Lagrangian (CEL) method; indeed some of these techniques are available in commercial software such as ABAQUS, and have been used for geotechnical problems (e.g. Kim et al. (2015)). Having said this, there is a school of thought that says adherence to mesh-based methods places a restriction of the development of numerical modelling, and there are many examples of mesh-free methods being developed, although most incur a greater computational cost to the FEM for standard problems at present (Heaney et al. 2010).

In this paper we are concerned with a relative newcomer to computational geotechnics, called the Material Point Method (MPM) which seems to offer advantages over the standard FEM for large deformation problems, without some of the complexities of rival approaches mentioned above. The MPM is of key and current interest in geotechnics having fea-

tured in Alonso's 2017 Rankine Lecture, and its use in geotechnics having been the feature of a major conference in the same year (Anura3D MPM Research Community 2017). In this paper we highlight a number of issues that geotechnical modellers might face when using the MPM and present recent solutions developed by the authors.

2 THE MATERIAL POINT METHOD

The MPM for solid mechanics was developed from an earlier method for fluids (the FLIP method) by Sulsky and co-workers (Sulsky et al. 1994). It is usually described in an explicit form where it is used for time-stepping analyses of problems with inertia and acceleration. It is however equally possible to formulate the MPM in implicit form (Guilkey and Weiss 2003) for quasi-static problems (usually of most interest in geotechnics) where to deal with non-linearity a total applied action is split into a number of substeps, in which each requires the solution of a linear system involving a stiffness matrix and an unknown vector of displacements.

The method is often referred to as an Eulerian-Lagrangian method (Muller & Vargas 2014) but this is not really correct; there are aspects of the method that make it look that way. In fact the calculations are just Lagrangian. In the MPM, a problem domain is defined with a set of material points (MPs, sometimes also referred to as particles). These MPs carry all the information relating to that location in the problem domain throughout a calculation, i.e. total displacement, strain, stress and if necessary other state variables required by a constitutive model. All calculations are however carried out on a finite element mesh (often referred to as a background grid) to which data are mapped back and forth from the material points. The feature in the MPM that is most attractive to those wishing to model large deformation is that the deformation of the problem domain is represented at the material points only and the background grid can be discarded after each time step. This means never having to calculate on a distorted grid, and also means that a regular structured grid can be reused each time, avoiding the overhead linked to unstructured mesh generation. A secondary but important aspect of the MPM, from the implementation point of view, is that much finite element technology can be seamlessly transferred to the MPM, especially items such as constitutive models and basis functions, reducing the overhead of code development and, perhaps, providing some confidence in the use of the method.

An important problem dealt with in the literature with the standard MPM is grid-crossing instability, which is a numerical artefact linked to a deformation pattern in which a material point leaves one grid element and enters another. In the standard MPM, where domain volume (or mass) is concentrated at a material point, this leads to a sudden change in stiffness of a grid element which causes non-physical numerical effects. This problem has been tackled by developing variants of the standard MPM where each material point carries a spatially-defined and potentially deforming volume (or mass) with it. Methods include the Generalised Interpolation MPM (Bardenhagen and Kober 2004, Charlton et al. 2017) and CPDI methods (Sadeghirad et al. 2011, Nguyen et al. 2017). While these variants effectively reduce grid-crossing instabilities they lead to additional complexities in calculations (especially the CPDI methods) and all suffer from the same issues which are covered in this paper.

3 THE MPM FOR GEOTECHNICS

It is clear there is keen and current interest in the use of the MPM in geotechnics as evidenced by an increasing number of papers describing its use for various geotechnical problems, for instance soil-structure interaction (Ma et al. 2014) and slope stability (Zabala and Alonso 2011), and a recent conference was devoted to MPM and geotechnics (Anura3D MPM Research Community 2017). In addition there are a number of survey papers, e.g. Sołowski and Sloan (2015). The MPM has also been developed to model coupled problems important in geotechnics, for example Jassim et al. (2013). The following sections cover three issues affecting use of the MPM or its variants for geotechnical analysis. The discussion relates primarily to our experiences with implicit MPM codes for elastic and elasto-plastic statics problems rather than explicit MPM with dynamics.

3.1 *Essential Boundary Conditions*

Essential (or Dirichlet) boundary conditions (BCs) are necessary to fully define a boundary value problem. They do not (usually) enter the weak form description of the problem but are subsidiary conditions that have to be incorporated. In the standard FEM, essential BCs are usually imposed directly, i.e. those degrees of freedom with essential BCs are treated differently, or the stiffness matrix is amended, as described in standard texts, e.g. Potts and Zdravković (1997). This is possible due to the Kronecker delta property of standard FE shape functions which delivers an *interpolation* of nodal unknowns. In contrast most weak-form based meshless methods, such as the element-free Galerkin method (Belytschko et al. 1994) have basis functions, often derived from moving least squares, that do not possess the Kronecker delta property and hence lead to *approximations* rather than interpolations. Consequently essential BCs have to be imposed indirectly (Fernández-Méndez and Huerta 2004).

The MPM (in all of its different flavours as mentioned above) has a problem with essential BCs of a

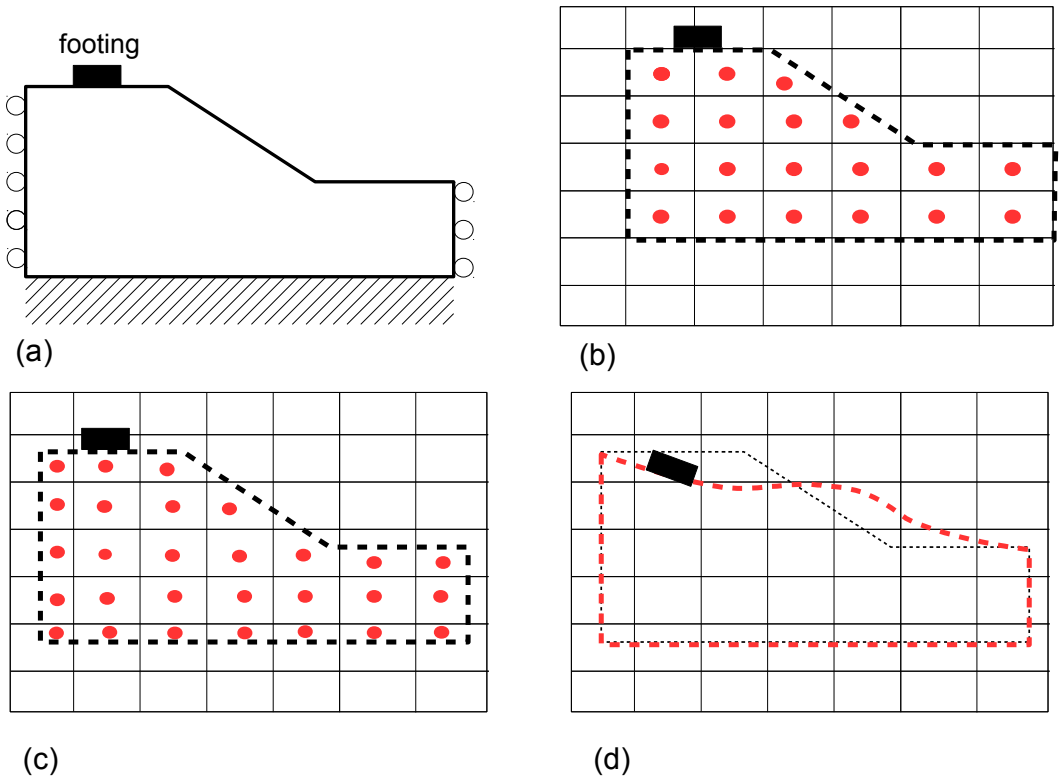

Figure 1: (a) slope stability problem geometry; (b) MPM solution requiring collinear grid and domain boundaries; (c) ideal MPM model with no requirement of collinear gird and domain geometry; (d) deformed domain. Red dots are the material points in each case.

slightly different nature. Consider Fig. 1 which shows a typical 2D plane strain discretisation of a slope stability problem, in which the vertical boundaries are subject to an essential boundary condition of zero displacement normal to the boundary while the bottom horizontal boundary is subject to an essential BC of full fixity or zero normal displacement. Providing the essential boundaries align exactly with the background grid (Fig. 1(b)), these conditions can be applied in the MPM directly just as in the standard FEM. All calculations are carried out on the background grid and therefore as the domain boundary coincides with edges of elements in the background grid for these three boundaries, there is exact coincidence with imposing essential BCs on the grid. However, if the problem domain boundary does not coincide with edges of elements in the background grid, an essential boundary condition cannot be applied this way. The example so far has concentrated on essential BCs which act as fixities in a boundary value problem, however geotechnical problems often require non-homogeneous essential BCs such as for the modelling of the footing shown at the top of the slope in Fig. 1. In this case, while it might be possible to arrange for the initial grid to align with the starting position of the footing, subsequent loading steps (in this case increments of applied displacement to the footing) would require grids to follow the predicted movements exactly, thus losing a key advantage of the MPM in that a regular grid, not connected to the domain geometry, can be used. While we now present a solution to this problem, in fact, Fig. 1 will be used to illustrate the other problems with the MPM on which this paper focusses in later sections. The issue outlined above is linked to a large body of emerging literature in computational solid mechanics on non-matching mesh methods which, as the name suggests, are numerical methods where solutions are calculated without matching the discretisation mesh to the problem domain, examples include immersed FE methods and the Finite Cell method (Ramos et al. 2015, Schillinger et al. 2012). In the case of the MPM, we have developed a new method for the imposition of essential BCs which removes any need for alignment of mesh edges and problem domain boundaries. It is based on Kumar and co-workers' *implicit boundary approach* (Kumar et al. 2008) and can be viewed as a form of penalty method of applying the essential BCs. In the method, essential boundaries are defined by signed distance functions ϕ_j where $\phi_j < 0$ indicates the exterior and $\phi_j > 0$ the interior of the problem domain for the jth boundary. Essential boundary (or Dirichlet) functions $d_j(\phi_j)$ are then defined for each boundary, which are equal to zero on the boundary and rise to unity a small distance δ on the domain side of the boundary. d_j are often simple discontinuous quadratic functions in ϕ_j. An example is shown

in Fig. 2 where the Dirichlet function is given by

$$d = \begin{cases} 0, & \phi < 0 \\ 1 - \left(1 - \frac{\phi}{\delta}\right)^2 & 0 \leq \phi \leq \delta \\ 1 & \phi > \delta \end{cases}. \quad (1)$$

At points where more than one essential boundary is active, i.e. at a domain corner, then the product of the $d(\phi_j)$ forms the essential boundary function and in general we write the net essential boundary at a point as

$$D_k = \prod_j d(\phi_j), \quad (2)$$

where k refers to the component of displacement defined at that boundary. D_k are then the components of the diagonal matrix $[D]$ used to redefine the trial functions for the grid elements as

$$\{u'\} = [D]\{u\} + \{u^a\} \quad (3)$$

where $[D] = diag(D_1, \ldots, D_{n_d})$ and n_d is the dimensionality. In Eqn 3, $\{u\}$ is the standard approximation for displacement in a finite element while $\{u^a\}$ is the essential boundary condition (i.e. zero for a fixed degree of freedom or non-zero for a prescribed displacement). Within the narrow band adjacent to the implicit boundary, the first term in Eqn 3 will be suppressed via the matrix $[D]$, enforcing the essential boundary condition in the second term. Substituting these trial functions and some suitable test functions into the standard weak form for equilibrium leads to expressions for the stiffness matrices of elements containing essential boundary conditions. Fig. 3 shows a grid element (cell) cut by an essential boundary. For this element the net stiffness matrix would be

$$[k^E] = [K_1] + ([K_2] + [K_2]^T) + [K_3], \quad (4)$$

where $[K_1]$ is the standard finite element stiffness matrix for the part of the element occupied by the problem domain and is obtained through the summation of the MP contributions, while $[K_2]$ and $[K_3]$ contain Dirichlet functions and their derivatives. The additional stiffness matrices $[K_2]$ and $[K_3]$ are effectively penalty terms imposing the essential BC crossing the element and their components are calculated by numerical integration in the bandwidth δ as shown in Fig. 3. It is straightforward to implement essential BCs which cut an element at an angle with respect to the element global coordinates; a transformation matrix is applied to components of the matrices forming $[K_2]$ and $[K_3]$. An example of the use of the approach is given in Fig. 4 where a rigid footing penetrates a unit distance into an elastic square domain of side 3 units. The roller sides and base are imposed as implicit homogeneous essential BCs while the footing is an implicit non-homogeneous essential BC. Full details of this approach for implementation of essential boundaries in the MPM are given in Cortis et al. (2017).

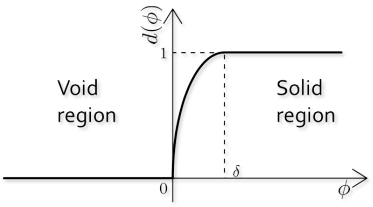

Figure 2: A Dirichlet function in 1D.

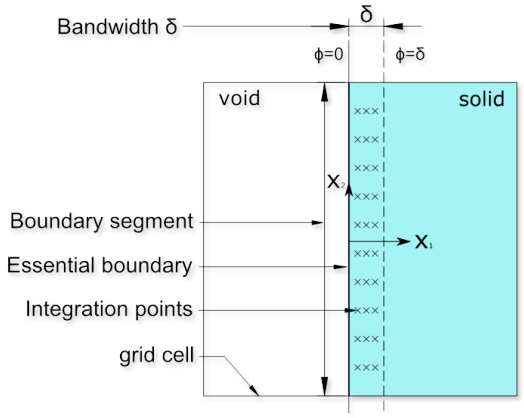

Figure 3: A single grid element (cell) crossed by an essential boundary condition

3.2 *Tracking domain boundaries*

Fig. 1(d) serves to illustrate another problem with the MPM for geotechnical problems, that of tracking evolving boundaries to a problem domain and application of traction (Neumann) boundary conditions. The former is particularly troublesome given that geotechnical engineers would like to use the MPM for problems in which this can be a crucial output, e.g. a key prediction for long runout landslides is the final surface profile of the disturbed material (e.g. Wang et al. (2016)). To date, researchers wishing to track free surfaces in an MPM analysis have been limited to determining the location of the edges of material point individual volumes which exist in GIMP and CPDI methods but not in the standard MPM. The best that these can deliver are piecewise linear edges (CPDI2) or stepped approximations (GIMP and CPDI1). As regards the application of traction boundary conditions this has been attempted in the past by placing loads at material points, which is clearly an inaccurate representation, particularly when wishing to exploit the capabilities of the MPM for large deformation problems.

In recent research undertaken at Durham, Bing (2017) describes a new method which can deliver both accurate tracking of domain boundaries and application of surface tractions in any variant of the MPM for arbitrary large deformations. A local cubic B-spline interpolation is used to represent the boundary based on a set of defined boundary material points. These can be additional material points (with near-zero volumes) placed on the boundaries or an outer layer of standard material points in the phys-

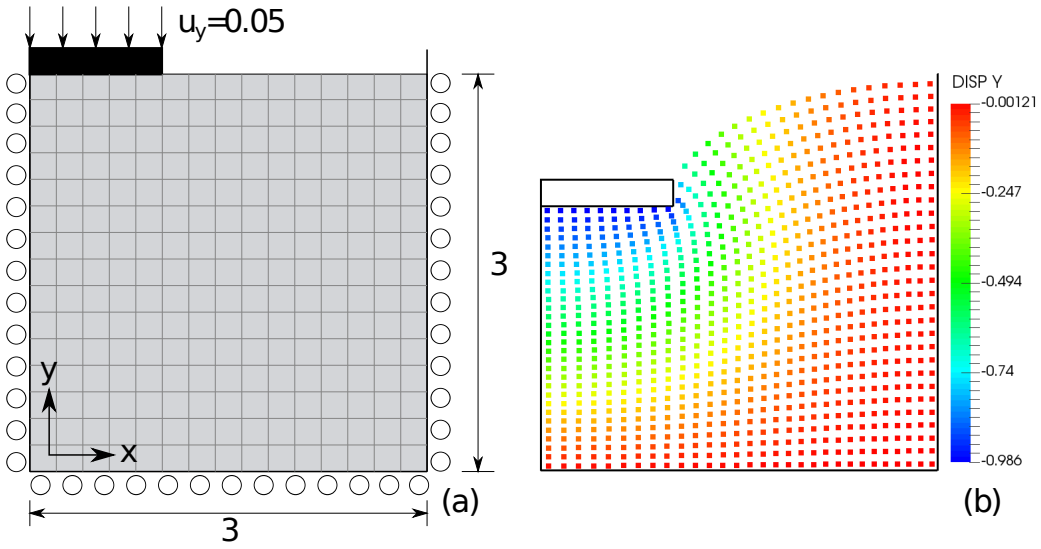

Figure 4: Rigid footing penetrating into an elastic domain: (a) problem definition, (b) deformation prediction using the MPM. (From Cortis et al. (2017))

ical domain. Spline segments are fitted between adjacent sampling points to calculate the B-spline control points and a suitable knot vector determined completing the description of the B-spline curve. Although fitting a curve globally to the boundary (Piegl & Tiller 1997) would result in higher continuity, it would not be capable of reproducing sharp corners which are important features in many geotechnical problem domains. Local fitting, as used here, constructs curves in a piecewise fashion so that only local data are used at each step, so a fluctuation in data only affects the curve locally. As regards spline order, a local cubic interpolation has a simpler formulation than the local quadratic interpolation (Piegl & Tiller 1997) and no special cases or angle calculations are needed.

Once an accurate boundary representation is in place we can consider how to apply boundary conditions. Essential boundary conditions on B-spline boundaries can be imposed with the implicit boundary method described above, with a few minor alterations. The application of tractions to a B-spline defined boundary is also straightforward with the only complexity arising in the integration required, as will be outlined now. In the standard FEM, nodal forces $\{f^t\}$ consistent with a surface traction $\{t\}$ on a surface $\mathrm{d}\Omega$ are obtained as

$$\{f^t\} = \int_{\partial\Omega} [M]^T \{t\}\, \mathrm{d}\Omega, \tag{5}$$

where $[M]$ contains the standard finite element shape functions. So for the case of the B-spline boundaries we have to consider how to carry out this integration. A pth-degree B-spline curve can be integrated numerically by using $(p-1)$th order Gauss quadrature. However, the local coordinate of 1D Gauss quadrature has a range of $[-1,1]$, whereas, the local coordinate of a B-spline curve has positive values only, therefore mapping between these two systems is required to complete the integration (in addition to the

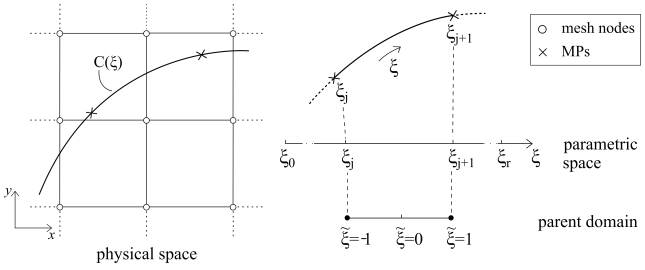

Figure 5: Physical and parametric spaces for numerical integration of boundary conditions.

standard map between the local and global coordinates, or physical space for isoparametric FEs). To allow for this, an additional space, called the *parent domain* is introduced over which quadrature takes place (Hughes, Cottrell, & Bazilevs 2005). Fig. 5 shows an illustration of the three spaces: the physical space, $\{x\}$, the parametric space, ξ, and the parent domain, $\tilde{\xi}$. In the physical space, the boundary geometry is defined in global coordinates. The parametric space contains the knots (local coordinates) which run along the curve and the parent domain is simply a local system where $\tilde{\xi} \in [-1,1]$ on which numerical integration is performed. To carry out the integration, the B-spline curve segment is pulled back from the physical space to the parametric space, i.e. the local coordinates (ξ_j and ξ_{j+1}) of the start and the end point of the segment are identified by using their global coordinates. A linear transformation between the parent domain, $\tilde{\xi} \in [-1,1]$, and the parametric space, $[\xi_j, \xi_{j+1}]$ maps the locations of Gauss points between these two spaces. In order that the integration can be completed, a Jacobian mapping is required between the parent and physical spaces between the Gauss quadrature lengths, which are defined over the local coordinates $\tilde{\xi} \in [-1,1]$, and the physical space. Due to the use of a two local coordinate systems, the Jacobian contains

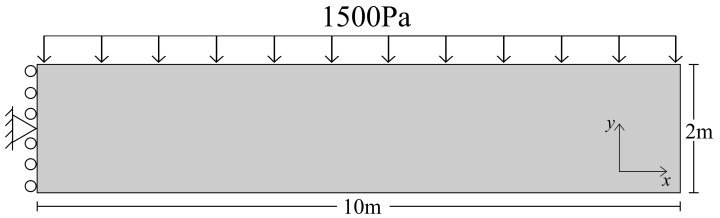

Figure 6: Cantilever beam geometry.

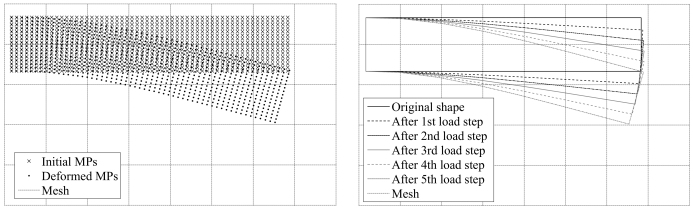

(a) Final deformation of the material points.

(b) Boundary visualisation after each load step.

Figure 7: Cantilever beam deformation.

two components

$$\{J_B\} = \left\{ \frac{dC}{d\tilde{\xi}} \right\} = \left\{ \frac{dC}{d\xi} \right\} \frac{d\xi}{d\tilde{\xi}} \tag{6}$$

where C is the B-spline curve defining a segment in the physical boundary. Applying Gauss quadrature to (5), we obtain

$$\{f^t\} \cong \sum_{i=1}^{n_{gp}} [M_i]^T \{t\}_i \, ||\{J_B\}_i|| w_i, \tag{7}$$

where n_{gp} is the number of Gauss points used to integrate over the segment within the background grid element, w_i is the weight associated with Gauss point i, $||(\cdot)||$ denotes the L2 norm of $(\cdot)$ and in this case the L2 norm of the boundary Jacobian, $\{J_B\}$, which maps the length of the boundary between the parent and physical spaces.

To illustrate the use of this method Fig. 6 shows an elastic cantilever beam of length 10 m and depth of 2 m is subjected to a constant pressure of 1500 Pa applied along the top boundary; a traction which remains perpendicular to the top surface of the cantilever throughout the analysis. A background grid with 1.5 m by 1.5 m elements is used, and the problem domain is discretised using 896 uniformly distributed standard material points. The outer layer of the material points are identified as the problem boundaries which are approximated using B-splines. The initial discretisation and the final deformed cantilever beam are shown in Fig. 7a. The advantage of this approach is that the boundaries can be tracked after each load step without plotting out all the material points (see Fig. 7b) and the deformed shape appears to be successfully captured by the B-spline approximation. Further examples and full details of this approach to accurately track domain boundaries and apply traction boundary conditions in the MPM are given in Bing et al. (2018) and Bing (2017).

3.3 *Volumetric Locking*

In the MPM the material points are integration points for the calculation of grid element stiffness, and since they are allowed to convect through the grid, they cannot provide the accuracy of an equivalent number of properly placed Gauss points. Consequently it is normal to use many more material points per grid element than the number required for accurate numerical integration. Combining this with the fact that the grid is usually comprised of low order elements, e.g. bilinear quadrilaterals in 2D, means that the method is susceptible to volumetric locking (resulting in over-stiff behaviour) when modelling near-incompressible materials. This volumetric locking is caused by excessive constraints placed on an element's deformation. That is, the constitutive model will require near-isochoric behaviour at the integration (or material) point's location within the element and each of these points places a constraint on the deformation of the element. A common technique to avoid volumetric locking in finite element methods is to use higher order elements with reduced Gaussian integration. However, this is not viable in MPMs since it is not known how many material points will be in any given element at a given load step. In the context of finite deformation solid mechanics, a number of formulations have been proposed to overcome volumetric locking in finite elements. (A review can be found in de Souza Neto et al. (2008)). The issue of volumetric locking in MPMs has received little attention to date with the notable exception of Mast et al. (2012) who investigated the issue of kinematic (volumetric and shear) locking in the standard MPM and developed a complex multi-field variational principle based approach which introduces independent approximations for the volumetric and the deviatoric components of the strain and stress fields.

For the MPM we have instead adopted the $\bar{F}$ approach hitherto applied to the standard FEM by de Souza Neto et al. (1996) for the following reasons: (i) unlike mixed approaches it does not introduce any additional unknowns into the linear system, (ii) it is simple to implement within existing finite element codes (and therefore also the MPMs), (iii) the approach can be used with any constitutive model and (iv) it does not introduce any additional *tuning* parameters into the code. In the $\bar{F}$ approach applied to standard FEM, the volumetric and deviatoric components of the deformation gradient are sampled at different locations. The deformation gradient becomes

$$\bar{F}_{ij} = \left(\frac{\det(F^0_{ij})}{\det(F_{ij})} \right)^{1/n_D} F_{ij}, \tag{8}$$

where n_D is the number of physical dimensions and

F^0_{ij} is the deformation gradient obtained from the deformation field at the centre of the element. Therefore the volumetric component of the deformation gradient for all of the Gauss points within an element is obtained from a single point, thus relaxing the volumetric constraint on the element when the material behaviour is near incompressible.

For the MPM, where we have large deformations, we adopt the incremental equivalent of (8), giving the $\bar{F}$ deformation gradient increment as

$$\Delta\bar{F}_{ij} = \left(\frac{\det(\Delta F^0_{ij})}{\det(\Delta F_{ij})}\right)^{1/n_D} \Delta F_{ij}, \tag{9}$$

where ΔF^0_{ij} is the volumetric component of the deformation gradient increment. It is straightforward to modify the standard material point method by replacing ΔF_{ij} with $\Delta\bar{F}_{ij}$ in the finite deformation formulation. This is because the shape functions are directly adopted from the finite element basis. However, it is more appropriate to use the geometric centre of the material points located within a given finite element rather than the centre of the element. This is due to two key reasons:

1. when a single material point is used to integrate the background grid cell the $\bar{F}$ deformation gradient, (9), equals the standard deformation gradient; and

2. when a background grid cell is only partially filled with material points the volumetric behaviour is centred on the physical region.

To demonstrate the performance of the MPM with the $\bar{F}$ approach results are presented for the analysis of a smooth square rigid footing bearing onto a 3D weightless elasto-plastic domain. Due to symmetry only a quarter of the physical problem is modelled and the footing has a half width of 0.5 m and the simulated domain is 5 m in length in each direction. The same material properties were adopted as (de Souza Neto et al. 2008) for their plane strain analysis of a rigid footing. The smooth footing was displaced vertically (z-direction) by 0.002m over 200 loadsteps and roller boundary conditions were imposed on the sides and the base of the domain. All of the boundary conditions were imposed using the implicit boundary method discussed above. A relatively coarse regular background grid of tri-linear hexahedral elements with $h = 0.2$ m was used to analyse the problem and the physical domain was discretised using 8 standard material points per background grid cell (125,000 material points in total). The force versus displacement response for the standard and $\bar{F}$ material point methods are shown in Fig. 8. The standard formulation locks and predicts an over-stiff response whereas the $\bar{F}$ formulation reaches a limit load, as expected for this type of analysis. Due to the small imposed displacement, material points do not cross

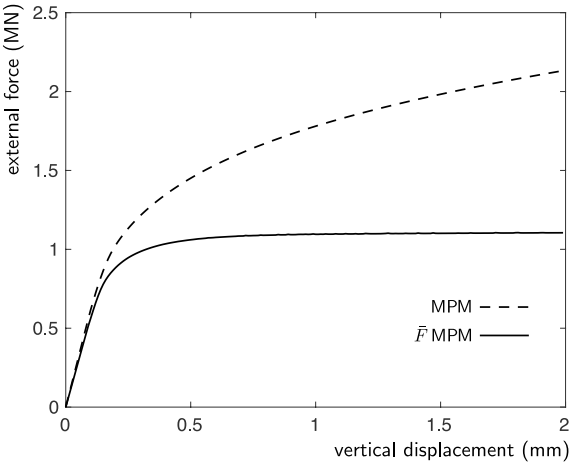

Figure 8: 3D footing: force displacement response for standard and $\bar{F}$ MPMs. (From Coombs et al. (2018)).

.

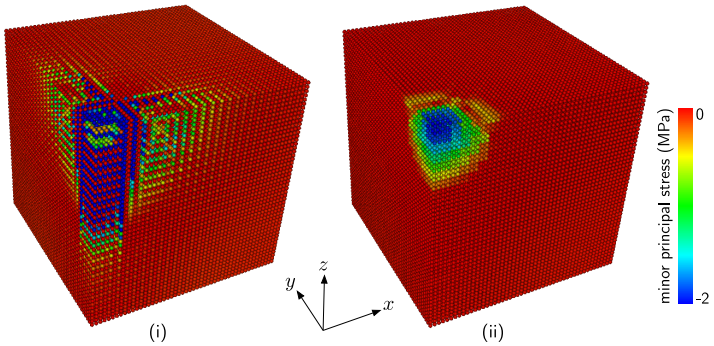

Figure 9: 3D footing: minor principal stress for (i) standard and (ii) $\bar{F}$ MPMs. (From Coombs et al. (2018)).

between background grid cells and both formulations give a smooth response. The minor principal (most compressive) stress distribution at the end of the analysis for the two formulations are shown in Fig. 9. The standard material point formulation contains spurious stress oscillations caused by volumetric locking. In particular, the column of material points underneath the footing oscillate between tensile and compressive stress states. The $\bar{F}$ formulation stress distribution shown in Fig. 9 (ii) demonstrates the correct compressive region underneath the footing, as shown by the blue-shaded particles. Full details of this approach to deal with locking in the MPM and other variants such as the GIMP method are given in Coombs et al. (2018).

4 CONCLUSIONS

In this paper we have attempted to summarise a number of issues with the use of the MPM that may afflict geotechnical analyses more than other applications for which it may be used. The literature to date shows that while these challenges have often been evident, many researchers have avoided tackling them head-on, especially in the area of imposition of essential boundary conditions. We have presented four

issues but have also presented solutions developed in our research group at Durham University. It is to be hoped that these solutions will provide useful to others attempting geotechnical modelling with the MPM in future.

ACKNOWLEDGEMENTS

Some of the work described in this paper has been undertaken for the UK EPSRC funded project *Seabed ploughing: modelling for infrastructure installation* (EP/M000362/1 & EP/M000397/1). The thirds author was supported by an EPSRC DTA Studentship during PhD study (grant ref EP/K502832/1) which has contributed to parts of this research.

REFERENCES

Anura3D MPM Research Community (2017). *First International Conference on the Material Point Method for Modelling Large Deformation and SoilWaterStructure Interaction*. `http://mpm2017.eu/home`.

Bardenhagen, S. & E. Kober (2004). The generalized interpolation material point method. *CMES- Computer Modeling in Engineering and Sciences 5*(6), 477–495.

Belytschko, T., Y. Y. Lu, & L. Gu (1994). Element-free Galerkin methods. *International Journal for Numerical Methods in Engineering 37*, 229–256.

Bing, Y. (2017). B-spline based boundary method for the material point method. MScR thesis, Durham University, UK.

Bing, Y., M. Cortis, T. Charlton, W. Coombs, & C. Augarde (2018). B-spline based boundary conditions in the material point method. *Computer Methods in Applied Mechanics and Engineering*. Under review.

Charlton, T. J., W. M. Coombs, & C. E. Augarde (2017). iGIMP: An implicit generalised interpolation material point method for large deformations. *Computers & Structures 190*, 108–125.

Coombs, W., T. Charlton, M. Cortis, & C. Augarde (2018). Overcoming volumetric locking in material point methods. *Computer Methods in Applied Mechanics and Engineering*. Accepted for publication.

Cortis, M., W. M. Coombs, C. E. Augarde, M. J. Brown, A. Brennan, & S. Robinson (2017). Imposition of essential boundary conditions in the material point method. *International Journal for Numerical Methods in Engineering*.

de Souza Neto, E., D. Perić, M. Dutko, & D. R. J. Owen (1996). Design of simple low order finite elements for large strain analysis of nearly incompressible solids. *International Journal of Soilids and Structures 33*, 3277–3296.

de Souza Neto, E., D. Perić, & D. Owen (2008). *Computational methods for plasticity: Theory and applications*. John Wiley & Sons Ltd.

Fernández-Méndez, S. & A. Huerta (2004). Imposing essential boundary conditions in mesh-free methods. *Computer Methods in Applied Mechanics and Engineering 193*, 1257–1275.

Guilkey, J. & J. Weiss (2003). Implicit time integration for the material point method: Quantitative and algorithmic comparisons with the finite element method. *International Journal for Numerical Methods in Engineering 57*, 1323–1338.

Heaney, C., C. Augarde, A. Deeks, W. Coombs, & R. Crouch (2010). Advances in meshless methods with application to geotechnics. In *Proc. NUMGE Trondheim*, pp. 239–244.

Hughes, T., J. Cottrell, & Y. Bazilevs (2005). Isogeometric analysis: Cad, finite elements, nurbs, exact geometry and mesh refinement. *Computer Methods in Applied Mechanics and Engineering 194*(39), 4135 – 4195.

Jassim, I., D. Stolle, & P. Vermeer (2013). Two-phase dynamic analysis by material point method. *International Journal for Numerical and Analytical Methods in Geomechanics 37*(15), 2502–2522.

Kim, Y., M. Hossain, D. Wang, & M. Randolph (2015). Numerical investigation of dynamic installation of torpedo anchors in clay. *Ocean Engineering 108*(Supplement C), 820 – 832.

Kumar, A. V., S. Padmanabhan, & R. Burla (2008). Implicit boundary method for finite element analysis using non-conforming mesh or grid. *International Journal for Numerical Methods in Engineering 74*(9), 1421–1447.

Ma, J., D. Wang, & M. Randolph (2014). A new contact algorithm in the material point method for geotechnical simulations. *International Journal for Numerical and Analytical Methods in Geomechanics 38*(11), 1197–1210.

Mast, C. M., P. Mackenzie-Helnwein, P. Arduino, G. R. Miller, & W. Shin (2012). Mitigating kinematic locking in the material point method. *Journal of Computational Physics 231*(16), 5351–5373.

Muller, A. L. & E. A. Vargas (2014). The material point method for analysis of closure mechanisms in openings and impact in saturated porous media. In *48th U.S. Rock Mechanics/Geomechanics Symposium, 1-4 June, Minneapolis, Minnesota*. American Rock Mechanics Association.

Nguyen, V. P., C. T. Nguyen, T. Rabczuk, & S. Natarajan (2017). On a family of convected particle domain interpolations in the material point method. *Finite Elements in Analysis and Design 126*(Supplement C), 50 – 64.

Piegl, L. & W. Tiller (1997). *The NURBS Book (2Nd Ed.)*. New York, NY, USA: Springer-Verlag New York, Inc.

Potts, D. & L. Zdravković (1997). *Finite element analysis in geotechnical engineering: Theory*. Thomas Telford.

Ramos, A., A. Aragn, S. Soghrati, P. Geubelle, & J.-F. Molinari (2015). A new formulation for imposing Dirichlet boundary conditions on non-matching meshes. *International Journal for Numerical Methods in Engineering 103*(6), 430–444.

Sadeghirad, A., R. M. Brannon, & J. Burghardt (2011). A convected particle domain interpolation technique to extend applicability of the material point method for problems involving massive deformations. *International Journal for Numerical Methods in Engineering 86*(12), 1435–1456.

Schillinger, D., M. Ruess, N. Zander, Y. Bazilevs, A. Duster, & E. Rank (2012). Small and large deformation analysis with the p- and b-spline versions of the finite cell method. *Computational Mechanics 50*(4), 445–478.

Sołowski, W. T. & S. W. Sloan (2015). Evaluation of material point method for use in geotechnics. *International Journal for Numerical and Analytical Methods in Geomechanics 39*(7), 685–701.

Sulsky, D., Z. Chen, & H. Schreyer (1994). A particle method for history-dependent materials. *Computer Methods in Applied Mechanics and Engineering 118*, 179–196.

Wang, B., M. A. Hicks, & P. J. Vardon (2016). Slope failure analysis using the random material point method. *Géotechnique Letters 6*(2), 113–118.

Zabala, F. & E. Alonso (2011). Progressive failure of Aznalcóllar dam using the material point method. *Géotechnique 61*(9), 795–808.